THE JOURNAL OF PHYSICAL CHEMISTRY B

Article

pubs.acs.org/JPCB

Ultrafast Dynamics of Nonequilibrium Electron Transfer in Photoinduced Redox Cycle: Solvent Mediation and Conformation Flexibility

Ya-Ting Kao, Xunmin Guo, Yi Yang, Zheyun Liu, Ali Hassanali, Qin-Hua Song,† Lijuan Wang, and Dongping Zhong*

Department of Physics, Department of Chemistry and Biochemistry, and Programs of Biophysics, Chemical Physics, and Biochemistry, 191 West Woodruff Avenue, The Ohio State University, Columbus, Ohio 43210, United States

ABSTRACT: We report here our systematic characterization of a photoinduced electron-transfer (ET) redox cycle in a covalently linked donor−spacer−acceptor flexible system, consisting of *N*-acetyl-tryptophan methylester as an electron donor and thymine as an electron acceptor in three distinct solvents of water, acetonitrile, and dioxane. With femtosecond resolution, we determined all the ET time scales, forward and backward, by following the complete reaction evolution from reactants to intermediates and finally to products. Surprisingly, we observed two distinct ET dynamics in water, corresponding to a stacked configuration with ultrafast ET in 0.7 ps and back ET in 4.5 ps and a partially folded C-clamp conformation with ET in 322 ps but back ET in 17 ps. In acetonitrile and dioxane, only the C-clamp conformations were observed with ET in 470 and 1068 ps and back ET in 110 and 94 ps, respectively. These relatively slow ET dynamics in hundreds of picoseconds all showed significant conformation heterogeneity and followed a stretched decay behavior. With both forward and back ET rates determined, we derived solvent reorganization energies and coupling constants. Significantly, we found that solvent molecules intercalated in the cleft of the C-clamp structure mediate electron transfer with a tunneling parameter (β) of 1.0−1.4 Å^{-1} and the high-frequency vibration modes in the product(s) couple with the back ET process, leading to the ultrafast back ET dynamics in tens of picoseconds. These findings provide mechanistic insights of nonequilibrium ET dynamics modulated by conformation flexibility, mediated by unique solvent configuration, and accelerated by vibrational coupling.

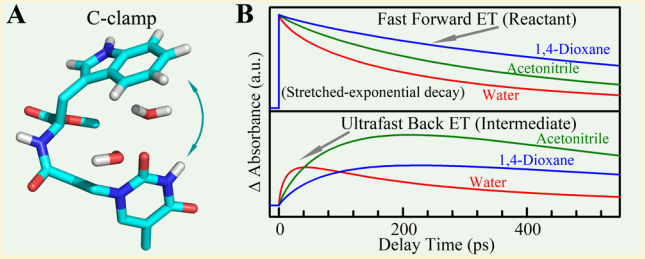

INTRODUCTION

Over the past decades, a large number of chemical systems, consisting of covalently linked electron donor (D) and acceptor (A), have been synthesized and investigated to examine electron transfer (ET) reactions[1−8] and theories[9−12] with controlled parameters of free energy gap (ΔG), reorganization energy (λ), and donor−acceptor coupling (J) or distance (r). These reactions were usually studied by changing one parameter while the other two parameters were fixed. For example, with the designed donor and acceptor, we can alter a series of distances (r) in a solvent or change different solvents (λ) with a fixed distance.[13−16] One extensively studied system is the "C-clamp" structure and particular solvent mediation, i.e., enhanced coupling J, was observed in the cleft of this C-shaped donor−spacer−acceptor configuration.[17−20] These dynamics usually follow a single exponential behavior with a defined ET rate dictated by the three parameters. However, when ET dynamics occur ultrafast on the similar time scales of solvent relaxation, the ET reactions are in nonequilibrium with local environments and the rates thus show significantly heterogeneous behaviors as predicted by theory[21−23] and observed in experiment.[24−27] This is particularly true for the recent observations in proteins.[28−34] When the linker between D and A is flexible and the distance varies on the similar time scales of ET, the ET dynamics must also be heterogeneous. If the linker fluctuation is further related to solvent viscosity, different solvents can have significant effects on ET dynamics, not only by reorganization energies but also D−A distances.

We here design a covalently linked electron donor−acceptor system consisting of an amino acid tryptophan analogue, *N*-acetyl-tryptophan methylester (NATME), and a nucleobase thymine (T), as the electron donor and acceptor, respectively (Scheme 1). Both the donor and acceptor are biomolecules and involved in protein−DNA recognition. Tryptophan is well-known to be an excellent electron donor upon excitation in UV region[35] and plays an important role in ET reactions in many biological processes.[36−40] We use a flexible linker between D and A, instead of a rigid spacer, to allow the system to adapt to various conformations with fluctuating D−A distances. Such a mobile D−A system is ideal to mimic flexible biological interactions and possible ET reactions between protein (tryptophan) and DNA (thymine).

We report here a systematic examination of the flexible donor−acceptor (NATME-T) system in various solvents with

Received: May 9, 2012
Revised: June 15, 2012
Published: June 26, 2012

ACS Publications © 2012 American Chemical Society

dx.doi.org/10.1021/jp304518f | *J. Phys. Chem. B* 2012, 116, 9130−9140

Scheme 1

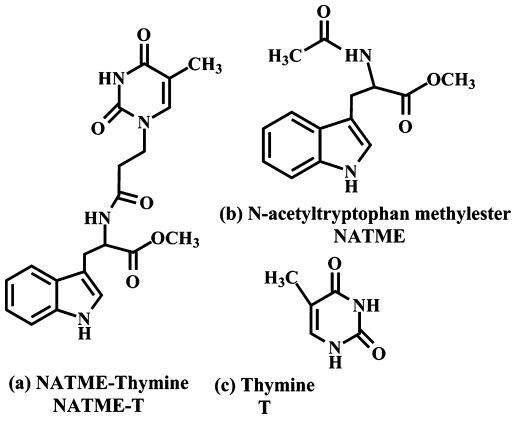

femtosecond (fs) resolution. With fs-resolved fluorescence and absorption spectroscopy, we study the photoinduced ET reactions and probe both forward and subsequent back ET dynamics by monitoring reactants, intermediates, and final products. We determine the actual time scales of each step in the redox cycle, and such results are essential to understanding the ET reactions with dynamic conformations in the normal Marcus region for forward ET and in the inverted region for back ET. Also, the ET dynamics of NATME-T will provide significant insights into the critical DNA-repair model reaction[41−43] that an electron from excited tryptophan is injected into thymine dimer in damaged DNA to restore the dimer to two normal thymine bases.

MATERIALS AND METHODS

Donor−Acceptor System. *N*-Acetyl-tryptophan methyl-ester (NATME) and a covalently linked electron donor−acceptor system (NATME-T), consisting of NATME as electron donor and thymine (T) as electron acceptor (Scheme 1), were synthesized, purified, and characterized as described previously.[42] The solvents, acetonitrile (ACN) and 1,4-dioxane (DIO), were of the highest commercially available purity and were used without further purification. Deionized water was obtained through the Millipore water purification system with a final resistivity of ∼18.2 MΩ·cm^{-1}. Thymine (T), *N*-acetyl-L-tryptophan amide (NATA), and L-tryptophan (Trp) were purchased from Sigma-Aldrich without further purification. Sample concentrations from 750 μM to 3 mM for NATME-T, NATME, T, NATA, and Trp were prepared in various solvents as needed and used in experiment.

Femtosecond Spectroscopy. All the femtosecond (fs)-resolved measurements were carried out by using fluorescence up-conversion and transient-absorption methods. The experimental layout has been detailed elsewhere.[44] Briefly, a femtosecond pulse after the two-stage amplifier (Spitfire, Spectra-Physics) has a temporal width of 110 fs centered at 800 nm with a pulse energy of more than 2 mJ and a repetition rate of 1 kHz. Half of the laser energy was used to pump an optical parametric amplifier (OPA-800C, Spectra-Physics) to generate the pulse at 570, 580, or 590 nm. Then, the pulse was frequency-doubled to generate the pump wavelengths at 285, 290, or 295 nm by a 0.2-mm-thick β-barium borate crystal (BBO, type I). The pump-pulse energy was attenuated to ∼140 nJ prior to being focused into the sample cell. For fluorescence up-conversion experiments, the fluorescence emission was collected by a pair of parabolic focus mirrors and mixed with a gating pulse from another half of fundamental pulses (800 nm, attenuated) in a 0.2 mm BBO crystal through a noncollinear configuration. The up-converted signal ranging from 228 to 253 nm was detected by a photomultiplier after passing through a double-grating monochromator. For transient absorption, the other half of laser energy was used to pump another optical parametric amplifier (OPA-800C or TOPAS, Spectra-Physics) to generate various probe wavelengths of 266−800 nm. The sensitivity of the transient-absorption method can reach 10^{-4}−10^{-5} of the absorbance change. The instrument response time is ∼450 fs for fluorescence detection and 250 fs for transient absorption. All experiments were done at the magic angle (54.7°). Samples were kept in stirring quartz cells during irradiation to avoid heating and photobleaching.

Characterization of Donor and Acceptor Lifetimes. Figure 1A shows the steady-state absorption and emission spectra of NATME in various solvents. NATME exhibits one absorption band with a peak at 279 nm in water, 281 nm in ACN, and 282 nm in DIO. The emission peak of NATME is at 352 nm in water and shifts to the blue side at 333 nm in ACN and 327 nm in DIO, consistent with the decreased trend of dielectric constants,[45] 78.5, 37.5, and 2.2 for water, ACN, and DIO, respectively.[46] Figure 1B shows the fluorescence transients of excited NATME, Trp, and NATA in water gated at 370 nm upon 285 nm excitation. The transients of excited NATME and NATA follow a single-exponential decay of 1.22 and 3.0 ns, respectively, while the transient of excited Trp exhibits a biexponential decay of 500 ps and 3.0 ns,[47] due to the amino- and carbonyl-quenching groups in proximity and thus resulting in proton and electron transfer reactions, respectively.[48] With an acetyl group (−$COCH_3$, R_1 in Figure 1B) attached to the amino group, the proton-transfer reaction is blocked. Hence, the excited NATME and NATA show a single lifetime. The observed distinct dynamics of excited NATME (1.22 ns) and NATA (3.0 ns) result from the substituted group (R_2 in Figure 1B) attached to the carbonyl group. With the stronger tendency to release an electron to the carbonyl group, the substituted group reduces the ability of the carbonyl group to accommodate an electron from the excited indole, resulting in a longer lifetime. These results are consistent with previous studies,[49] showing the quenching order being $CH_3CO-\underline{CH_3}$ > $CH_3CO-\underline{OH}$ ≈ $CH_3CO-\underline{OCH_3}$ > $CH_3CO-\underline{NH_2}$ ≈ $CH_3CO-\underline{O^-}$.

Figure 1C shows the fluorescence transients of excited NATME in water, ACN, and DIO gated at 370 and 320 nm. At 370 nm emission, the transients exhibit a lifetime of 1.22, 3.02, and 2.77 ns in water, ACN, and DIO, respectively. Interestingly, the dynamics of excited NATME in ACN is slowest. ACN has the largest static dipole moment of 3.92 D, much bigger than those of water (1.85D) and DIO (0.45D).[46] The ACN molecules around NATME in the solvation shell with such large dipole moments probably reduce the electrophilicity of the carbonyl group, resulting in a slower electron-transfer dynamics and thus a longer lifetime. When we gated the blue side of the emission peak, we observed a mixture of solvation dynamics and lifetime emission. For example, at 320 nm emission, the transient shows an extra ultrafast decay of 1.64 ps (62%) in water. In ACN and DIO, such an ultrafast decay in 1−4 ps (15−25%) is also observed in the 320 nm transients. Thus, to accurately determine the ET dynamics (rate) between NATME and T, we must detect the fs-resolved fluorescence dynamics at the emission peak or longer wavelengths.

dx.doi.org/10.1021/jp304518f | J. Phys. Chem. B 2012, 116, 9130−9140

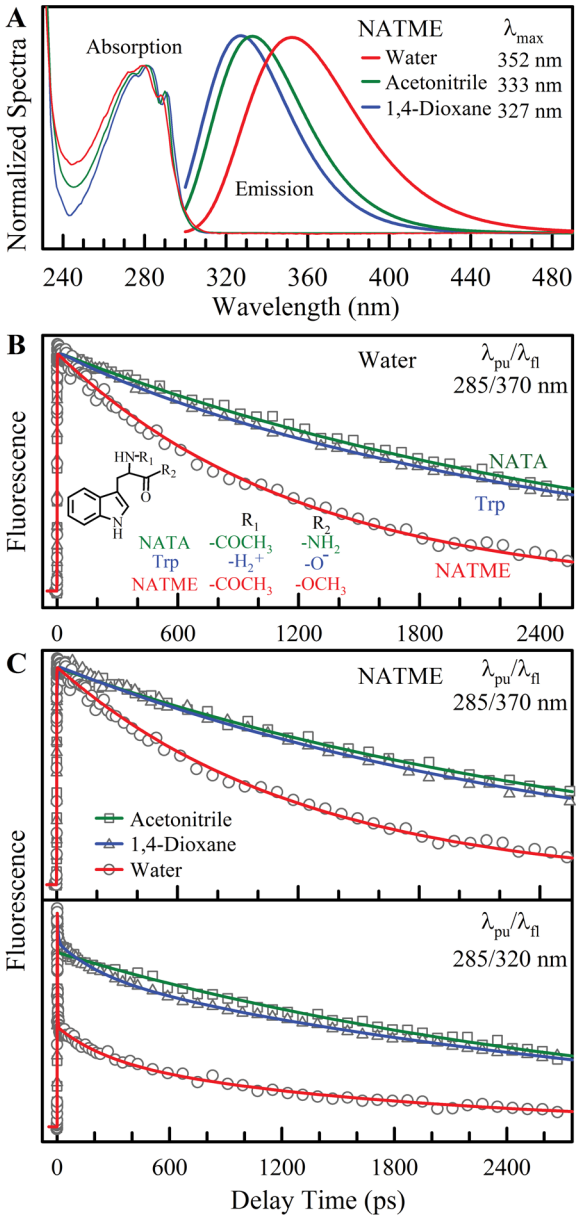

Figure 1. Steady-state spectra and ultrafast fluorescence dynamics of NATME and its derivatives. (A) Normalized absorption (thin line) and emission (thick line) spectra of NATME in water (red), acetonitrile (green), and 1,4-dioxane (blue). Note that the emission spectra in solvents with lower dielectric constants are blue-shifted. (B) Femtosecond-resolved fluorescence transients of NATME (red), Trp (blue), and NATA (green) in water, gated at 370 nm upon 285 nm excitation. With an acetyl group ($-COCH_3$, R_1) attached to an amino group, the excited NATME and NATA show a single lifetime while excited Trp exhibits two lifetimes. (C) Femtosecond-resolved fluorescence transients of NATME in water (red), acetonitrile (green), and 1,4-dioxane (blue), gated at 370 (upper) and 320 nm (lower) upon 285 nm excitation. Note that an extra decay component in a few picoseconds was observed at 320 nm transients due to solvation dynamics.

At 285 nm excitation, both NATME*-T and NATME-T* are generated and contribute to the 370 nm fluorescence signal (Figures 1A and 2, inset). Thus, we further examined the dynamics of excited thymine, and Figure 2 shows the fluorescence transients of excited thymine (T*) alone gated at 370 nm in three solvents. We observed ultrafast dynamics of

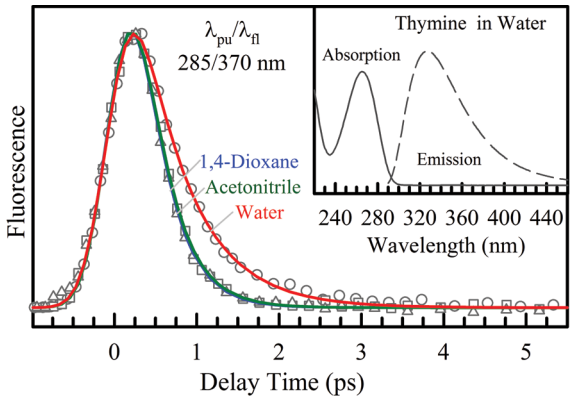

Figure 2. Femtosecond-resolved fluorescence transients of thymine (T) in water (red), acetonitrile (green), and 1,4-dioxane (blue), gated at 370 nm upon 285 nm excitation. Inset: steady-state absorption and emission spectra of thymine. Note that the integrated fluorescence is very weak due to the extremely small fluorescence quantum yield and ultrafast dynamics of internal conversion.

0.60, 0.34, and 0.32 ps in water, ACN, and DIO, respectively. The 0.60 ps in water is slightly faster than the dynamics of excited thymidine in aqueous solution, 0.7 ± 0.12 ps.[50] Typically, with attachment on the N1 position of thymine, the dynamics becomes slower and the quantum yield increases. Such ultrafast deactivation of excited pyrimidine bases presumably results from the rapid internal conversion through conical intersection(s) (CIs).[51] Because of the ultrafast lifetime of T*, if the ET occurs in NATME-T* between NATME and T*, the dynamics must also be ultrafast on the subpicosecond time scale.

RESULTS AND DISCUSSION

Electron Transfer, Stretched Behavior, and Conformation Flexibility. Figure 3 shows the fluorescence transients of NATME-T gated at 370 nm emission in three solvents. The fluorescence transients of excited NATME-T become much faster, compared with those of NATME* in Figure 1C (upper panel). Except for the initial ultrafast decay in less than 1 ps, the

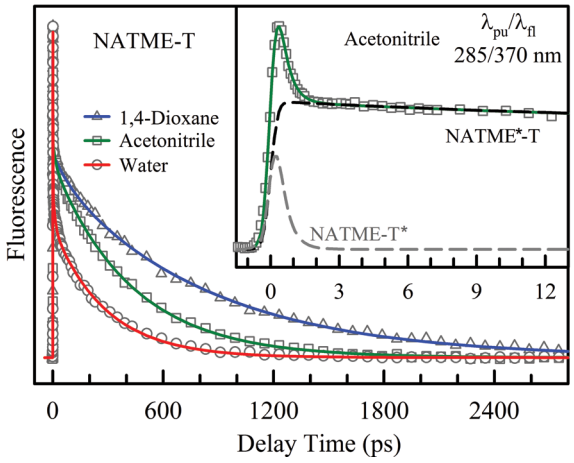

Figure 3. Femtosecond-resolved fluorescence transients of NATME-T in water (red), acetonitrile (green), and 1,4-dioxane (blue), gated at 370 nm upon 285 nm excitation. Inset: the deconvolution of 370 nm transient of NATME-T in acetonitrile showing both NATME*-T and NATME-T* dynamics.

dx.doi.org/10.1021/jp304518f | J. Phys. Chem. B 2012, 116, 9130−9140

transients can be best represented by a stretched-exponential decay, $Ae^{-(t/\tau)^{\beta}}$, or a double-exponential decay; see Table 1.

Table 1. Time Scales Obtained for the Forward ET Dynamics of NATME*-T and NATME* Lifetimes in Three Solvents Determined by Fluorescence Transients

	water	ACN	DIO
NAMTE* $(k_d)^{-1}$	1.22 ns	3.02 ns	2.77 ns
NAMTE*-T $(k_d + k_{ET})^{-1}$			
bi-exponential fit	13 ps (22%)	16 ps (9%)	7 ps (6%)
	285 ps (78%)	422 ps (91%)	829 ps (94%)
stretched-single-exponential fit	212 ps (β = 0.72)	376 ps (β = 0.85)	722 ps (β = 0.87)
	$\langle\tau\rangle$ = 261 ps	$\langle\tau\rangle$ = 407 ps	$\langle\tau\rangle$ = 771 ps
electron transfer $(k_{ET})^{-1}$	322 ps	470 ps	1068 ps

Specifically, in water, the transient can be fitted with τ = 212 ps and β = 0.72, besides the initial ultrafast decay in 0.78 ps. The average lifetime, $\langle\tau\rangle = (\tau/\beta)\Gamma(1/\beta)$, is about 261 ps. Similarly, the dynamics can be fitted by τ = 376 ps and β = 0.85 with an average lifetime of 407 ps in ACN and by τ = 722 ps and β = 0.87 with an average lifetime of 771 ps in DIO, except the rapid decay components of 0.40 and 0.55 ps, respectively. Since the solvation dynamics of three solvents are much faster than the stretched dynamics observed here, the intramolecular ET dynamics between NATME and T would follow a single exponential behavior, if there was a rigid configuration between indole and T moieties. However, the indole and thymine are connected by seven single bonds and thus the structure of NATME-T must be very flexible, resulting in a heterogeneous ET process with a stretched-exponential behavior. In our recent studies of ET dynamics at the active site of enzyme photolyase,[28,30,31] the observed ET dynamics showed a similar stretched behavior, not due to the flexible donor−acceptor conformation but resulting from the active-site solvation. The ET dynamics occurred on the similar time scales of active-site relaxation, leading to a heterogeneous ET process. Here, it is the conformation fluctuation, not the solvation relaxation, to have a distribution of configurations and to make the ET dynamics heterogeneous.

The potential for NATME/NATME$^+$ is +1.05 V vs NHE[52] and for T/T$^-$ is about −2.05 V vs NHE.[53] Knowing the 0−0 transition energy at ∼300 nm (4.13 eV),[54] we obtained a net ΔG of −1.03 eV. Thus, the intramolecular ET between the two moieties is energetically favorable. The observed dynamics in hundreds of picoseconds must result from ET from NATME* to T to form the NATME$^+$-T$^-$ ionic pair, and the stretched behavior must reflect the dynamic heterogeneity of flexible conformations. After taking the lifetime of NATME* into account, the final time scales of ET from NATME* to T are 322 ps in water, 470 ps in ACN, and 1068 ps in DIO (Table 1). On the other hand, with 285 nm excitation, NATME-T* is also generated. The observed initial ultrafast decay (<1 ps) is on the similar time scale as the dynamics of T* alone (Figure 2) in all three solvents. Thus, the initial dynamics could just be the dynamics of the T* moiety in NATME-T. As shown in the inset in Figure 3, the fluorescence transient of excited NATME-T in ACN is the sum of the dynamics of NATME*-T and NATME-T*, as also confirmed by our transient-absorption measurements below. However, in Figure 3, we clearly observed that the initial ultrafast decay component is more dominant in water than in ACN and DIO. Under identical experimental conditions with the same concentration, the fluorescence transient signal of T* in water is about half of the ultrafast decay component of excited NATME-T, indicating that besides the T* dynamics of excited NATME-T, there must be another ultrafast process in excited NATME-T. This ultrafast process must be related to a reaction between NATME and T upon excitation. As also shown in the transient-absorption measurements below, this process is an ultrafast ET reaction of NATME*-T in a stacked configuration with van der Waals contact between NATME and T. Also, this stacked configuration is only observed in water, not in solvents of ACN and DIO.

Back Electron Transfer, Stacked Configuration, and Redox Cycle. After ET, the redox pair of NATME$^+$-T$^-$ must proceed to charge recombination to restore the original form of NATME-T and finish the ET redox cycle. Thus, we further used the transient absorption method to detect all putative intermediates and products to obtain the back electron transfer (BET) dynamics. It is known that the indole radical cation has absorption peaks around 580 and 330 nm,[55] and Figure 4 shows the absorption transients probed at 580 nm in three solvents. Similarly, under the identical experimental conditions with the same concentrations, we did not observe noticeable ultrafast decay components of T* at 580 nm probe wavelength in three solvents, and thus, as shown in the inset of Figure 4, the transient reflects the sum of two dynamic processes of NATME*-T and its consequent charge-separated intermediate, NATME$^+$-T$^-$. Specifically, using the same stretched β value, in ACN, we observed an average decay component in 460 ps (100%) for NATME*-T and a formation and decay component (12%) in 460 and 110 ps, respectively, for NATME$^+$. The observed time scale of 110 ps is important and represents the BET dynamics between NATME$^+$ and T$^-$. In DIO, we observed the BET process on a similar time scale of 94 ps with an amplitude of 9.0%. The observed small amplitudes of NATME$^+$ are due to the slower formation and faster decay, resulting in less accumulation of intermediate NATME$^+$ and also an apparent reverse kinetics.

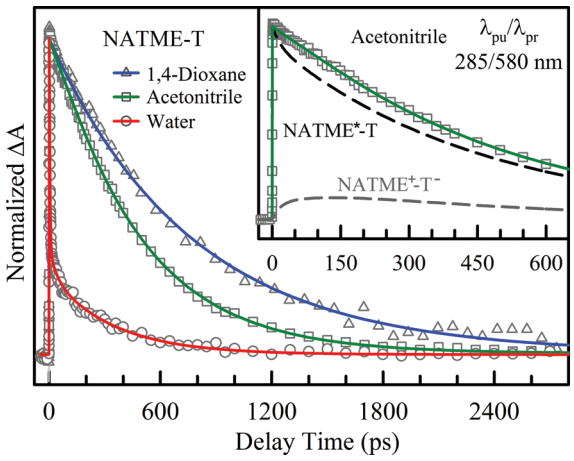

Figure 4. Femtosecond-resolved absorption transient of NATME-T in water (red), acetonitrile (green), and 1,4-dioxane (blue), probed at 580 nm upon 285 nm excitation. Inset: the deconvolution of 580 nm absorption probing of NATME-T in acetonitrile showing both NATME*-T and the intermediate NATME$^+$-T$^-$ dynamics. Note that a dominant ∼4 ps component was observed in water, absent in the other two solvents.

dx.doi.org/10.1021/jp304518f | J. Phys. Chem. B 2012, 116, 9130−9140

Strikingly, in water, we observed a dominant decay component in ~4 ps, absent in other two solvents (Figure 4). Also, this 4 ps decay component is not observed in NATME* or T* alone at 580 nm probing and thus is not a deactivation process of NATME* or T*. The dynamics must relate to the intermediate $NATME^+$ of the ET reaction(s) between NATME and T upon excitation. Thus, the extra ultrafast process (~0.78 ps) observed in the 370 nm fluorescence transient and 4 ps decay dynamics here are most likely to be ET and BET processes, respectively, between NATME and T moieties. For ET to occur on such a short time scale, the donor and acceptor must be in close contact. Because of the flexible linkage between NATME and T, NATME-T in water can also adapt a stacked conformation with two rings in proximity, which allows ET to occur in hundreds of femtoseconds. Thus, the ultrafast fluorescence decay in 0.78 ps is a sum of four processes: the ET dynamics of NATME*-T and partially NATME-T* in the stacked configuration and the moiety T* decays mainly from the open (C-clamp shape, see below) and partially from the stacked NATME-T* conformations. The 4 ps decay component is from the $NATME^+$ dynamics from both ET dynamics of stacked NATME*-T and NATME-T*. Figure 5 shows the detailed analyses of the

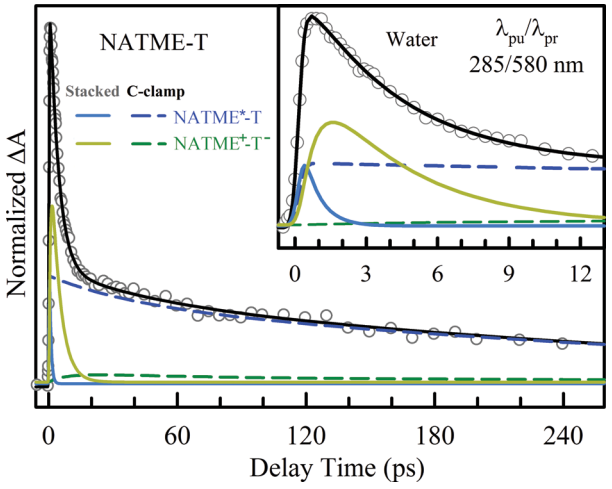

Figure 5. Detailed analyses of the 580 nm absorption transient of NATME-T in water upon 285 nm excitation. The 580 nm transient is a sum of the dynamics of NATME*-T (blue) and the intermediate $NATME^+$-T^- (green) from both stacked (solid line) and open (dashed line) conformations.

580 nm transient decomposition into four components: For the stacked form, the ultrafast ET dynamics (0.68 ps and 100%) of NATME*-T and the formation (0.68 ps) and decay (~4 ps) of $NATME^+$ (144%) from both NATME*-T and NATME-T*; and for the C-clamp form, the ET dynamics in 350 ps (100%) and the formation (350 ps) and decay (17.5 ps) of $NATME^+$ (5%), again a reverse kinetics and less accumulated intermediate of $NATME^+$ in the open conformation.

We further examined the ET dynamics in two forms of C-clamp and stacked configurations using a wide range of probing wavelengths from visible 800 nm to UV 266 nm. Figure 6 shows a series of the typical transients with the similar analyses as for the 580 nm transient, and in insets, we showed the decomposition of the transients for three wavelengths. For the probing at 800 and 330 nm, we showed the ET dynamics of both stacked and C-clamp forms and the total intermediate(s)

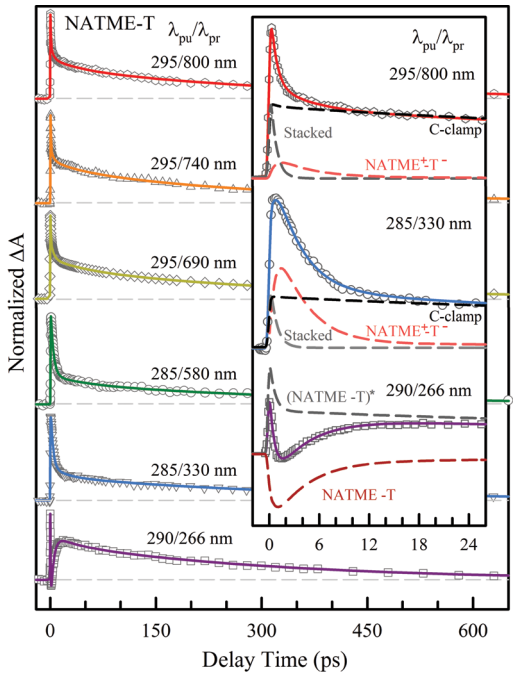

Figure 6. Femtosecond-resolved absorption transients of NATME-T in water for various pump/probe schemes. Inset: the deconvolution of 295/800 (top), 285/330 (middle), and 290/266 nm (bottom) transients. At 266 nm probing, we observed not only (NATME-T)* dynamics from both the stacked and open forms but most importantly the NATME-T recovery dynamics. In the stacked form, the coupled solvation and ET dynamics is 0.6−0.75 ps and the back ET takes 3.5−4.5 ps. In the open form, the ET dynamics is 328−355 ps and the back ET takes 14.7−18.0 ps.

dynamics of $NATME^+$-T^- of both forms. For the stacked form, we observed the ET dynamics in 0.69 and 0.75 ps and the charge-separated intermediate(s) decay in 4.3 and 3.6 ps. For the C-clamp form, the ET dynamics occur in 340 and 355 ps and intermediate(s) decay in 15.7 and 18 ps. We observed a larger signal of $NATME^+$-T^- at 330 nm due to the stronger absorption of $NATME^+$. At 266 nm probing, we showed the total ET dynamics of (NATME-T)* and total recovery signal of NATME-T of both forms. The intermediate signals at this wavelength are very small and negligible. Significantly, we observed one ground-state recovery component NATME-T in 4.3 ps and this recovery signal must be from the stacked BET. The successful detection of the ground-state recovery unambiguously showed the existence of the stacked conformation with ET in 0.60−0.75 ps and BET in 3.6−4.5 ps in water upon excitation. For the C-clamp form of NATME-T, the ET occurs in 328−355 ps and the BET in 14.7−18.0 ps. All time scales of ET and BET are listed in Table 2. In all probing wavelengths, we observed the ratio of the stacked to open conformations being 62 to 38%.

In Figure 7, we show our 25 ns molecular dynamics (MD) simulations on conformation fluctuations in the ground state with the center-to-center distances of two rings (indole and thymine) in water and ACN. Clearly, the structure of NATME-T is very flexible. Surprisingly, in water, we observed a significant distribution of the stacked conformation with the center-to-center distance at ~4 Å and the possible open form is actually a partially folded configuration in a C-clamp shape with the center-to-center separation at ~7.0 Å. However, in ACN, although the MD results showed a wide distribution of

dx.doi.org/10.1021/jp304518f | J. Phys. Chem. B 2012, 116, 9130−9140

Table 2. Time Scales Obtained for the Back ET Dynamics of NAMTE$^+$-T$^-$ in Three Solvents Determined by Absorption Transients

	water					ACN	DIO
probing wavelength	800 nm	740 nm	690 nm	580 nm	330 nm	580 nm	580 nm
			Open Form				
NATME*-T	340 ps (33%)	328 ps (34%)	345 ps (32%)	350 ps (19%)	355 ps (19%)	460 ps (100%)	850 ps (100%)
NAMTE$^+$-T$^-$	**15.7 ps (<1%)**	**14.7 ps (<1%)**	**17.1 ps (<1%)**	**17.5 ps (1%)**	**18.0 ps (1%)**	**110 ps (12%)**	**94 ps (9%)**
			Stacked Form				
NATME*-T/NATME-T*	0.69 ps (55%)	0.60 ps (56%)	0.62 ps (52%)	0.68 ps (32%)	0.75 ps (31%)		
NAMTE$^+$-T$^-$	**4.3 ps (12%)**	**4.2 ps (10%)**	**4.5 ps (16%)**	**4.0 ps (48%)**	**3.6 ps (49%)**		

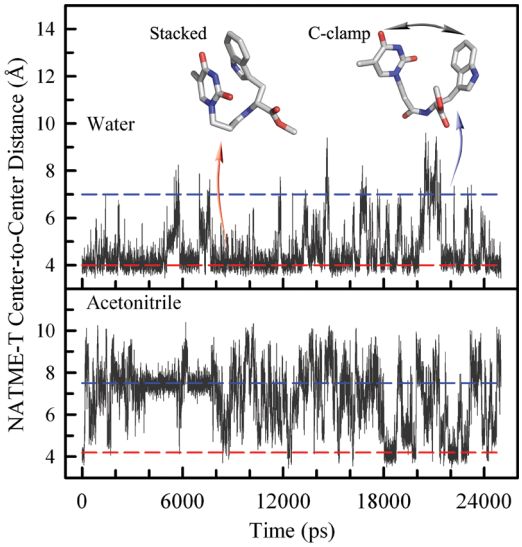

Figure 7. Trajectory fluctuations of the center-to-center distances between the indole ring and the thymine ring from our 25 ns molecular dynamics (MD) simulations for NATME-T in water (upper) and acetonitrile (lower). The red dashed line indicates that the two rings are in close proximity, a stacked form. The blue dashed line represents a partially folded C-clamp form. The gray arrow between two rings shows possible fluctuations, resulting in dynamic heterogeneity of ET reactions.

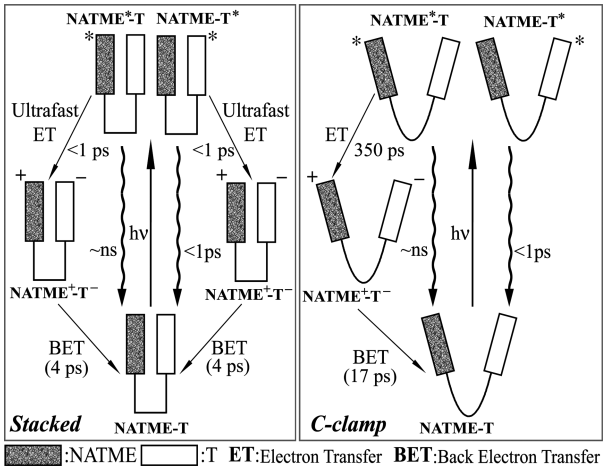

Figure 8. A kinetic model of photoinduced ET redox cycle for NATME-T in water. In the stacked form, both NATME*-T and NATME-T* show ultrafast ET (<1 ps) and subsequent back ET in ~4 ps to restore the original NATME-T. In the C-clamp form, due to rapid deactivation of NATME-T*, the ET process from NATME to T* is negligible. The ET dynamics of NATME*-T takes hundreds of picoseconds with subsequent back ET in tens of picoseconds. Only C-clamp conformations were observed in acetonitrile and dioxane with the similar ET time scales.

conformations with a possible C-clamp form at ~7.5 Å, we did not observe any ultrafast ET and BET processes experimentally and thus NATME-T may only adapt C-clamp conformations in ACN, as well as in DIO. More MD simulations on the excited state would be more helpful to examine the excited-state equilibrated configurations and fluctuations and the dynamics of conformational transitions from the ground to excited states. Figure 8 shows the complete photoinduced redox cycle for two forms of stacked and C-clamp configurations and related ET and BET processes in water. In ACN and DIO, NATME-T adapts the only C-clamp conformations with a heterogeneous distribution of configurations. The photoinduced ET dynamics show a stretched behavior due to the similar time scales of ET (hundreds of picoseconds) and conformation fluctuations. However, the BET dynamics is faster within 100 ps. Besides the C-clamp conformation in water, NATME-T also adapts a stacked conformation with a significant percentage (68%) and two moieties are in close proximity. The ET dynamics are ultrafast in less than 1 ps and the BET occurs in a few picoseconds. The accurate determination of time scales of forward ET, back ET, and the conformation dynamics in the complete redox cycle of excited NATME-T in three distinct solvents are critical to developing the deep understanding of ET dynamics in photoinduced ET chemical systems with flexible structures.

Reorganization Energy, Coupling Scheme, and Solvent Mediation. For NATME-T in water, we observed the forward ET in ~0.7 and ~350 ps and back ET in ~4 and ~17 ps for the stacked and C-clamp conformations, respectively. The distinct ET dynamics must result from the different conformations, leading to the various donor−acceptor distances, coupling schemes, and reorganization energies. In solvents of ACN and DIO, the forward ET is in ~460 ps and ~1 ns and the back ET in ~110 and ~95 ps, respectively. The different dynamics are due to the different solvent polarity, resulting in the various driving forces, configurations (distances), and reorganization energies. According to the Marcus theory[11] and semiempirical formula,[56] the ET rate can be expressed as follows:

$$\log k = 13 - A - 3.1\frac{(\Delta G + \lambda)^2}{\lambda},$$
$$A = \beta(r_{DA} - r_0)\log e = 0.434\beta(r_{DA} - r_0) \quad (1)$$

where k is the ET rate in s^{-1}, A is related to the electronic coupling term, ΔG is the total free energy of the reaction in eV, λ is the reorganization energy in eV, β here is the empirical ET tunneling parameter in $Å^{-1}$, and r_{DA} is the separation distance

dx.doi.org/10.1021/jp304518f | J. Phys. Chem. B 2012, 116, 9130−9140

in Å. r_0 is the van der Waals distance at 3.0 Å for calculating ET rates at long tunneling distances. For different tunneling schemes, the β parameters are different. For tunneling through covalent bonds, β = 0.71 Å^{-1}; in proteins, β = 1.0−1.4 Å^{-1}; in water, β = 1.55−1.65 Å^{-1}; and through space (vacuum-type), β = 2.9−4.0 Å^{-1}.[57] We can also write eq 1 in the Marcus semiclassical ET expression[11] and then calculate the coupling constant (J) if we know the free energy and reorganization energy.

$$k_{ET} = \sqrt{\frac{4\pi^3}{h^2\lambda k_B T}} J^2 \times 10^{-3.1(\Delta G+\lambda)^2/\lambda} \quad (2)$$

The driving forces (free energies) for photoinduced FET and subsequent BET can be determined by the following eqs 3 and 4, respectively.[58]

$$\Delta G_{FET} = E_{ox}(D/D^+) - E_{red}(A/A^-) - E_{0-0} - \frac{e^2}{4\pi\varepsilon_0\varepsilon_s r_{DA}} \quad (3)$$

$$\Delta G_{BET} = E_{red}(A/A^-) - E_{ox}(D/D^+) + \frac{e^2}{4\pi\varepsilon_0\varepsilon_s r_{DA}} \quad (4)$$

where E_{ox} and E_{red} are the redox potentials of the donor D and acceptor A, respectively, in corresponding solvent media, which already include solvation effects. E_{0-0} is the 0−0 transition energy from the ground-state S_0 to the first excited-state S_1. The last term in both equations accounts for the Coulombic interaction between D^+ and A^- with the electronic charge e and the static dielectric constant ε_s. At 25 °C, the dielectric constants of water, ACN, and DIO are 78.5, 37.5, and 2.2 and the resulting Coulombic interaction energies with the C-clamp form at r_{DA} = 7.0 Å are −0.026, −0.055, and −0.93 eV, respectively. Thus, in polar solvents, the Coulombic interaction energy is negligible, but in nonpolar solvents, it is significant. The solvent reorganization energy, especially for polar media, could be estimated from the following equation[11]

$$\lambda_s = \frac{e^2}{4\pi\varepsilon_0}\left(\frac{1}{2r_D} + \frac{1}{2r_A} - \frac{1}{r_{DA}}\right)\left(\frac{1}{\varepsilon_{op}} - \frac{1}{\varepsilon_s}\right) \quad (5)$$

where r_D and r_A are the ionic radii of the donor and acceptor, respectively, and ε_{op} is the optical (high frequency) dielectric constants of solvents. Typically, the λ_s value becomes smaller with a decrease in solvent polarity and it is usually underestimated in nonpolar solvents. Using radii of 2.2 Å[59,60] for both r_D (indole) and r_A (thymine) and a distance of 7.0 Å for r_{DA}, we estimated the λ_s values of 2.46, 2.36, and 0.24 eV for NATME-T in water, ACN, and DIO, respectively. The λ_s values in water and ACN could be overestimated comparing with the experimental results of ET between two organic compounds with various separation distances in ACN where λ_s is in a range of 0.5−1.9 eV.[61,62] The λ_s value in DIO might be underestimated given that λ_s was reported to be larger than 0.18 eV in nonpolar benzene.[63] Thus, the estimated λ_s values here were only used as the references in our calculations below.

In water, the free energies of ΔG_{FET} and ΔG_{BET} for the photoinduced NTAME-T redox cycle are −1.03 and −3.1 eV, respectively. For both the stacked (r_{DA} = 4.0 Å) and C-clamp (r_{DA} = 7.0 Å) forms, with knowing both the forward and back ET rates together and given the constraint that the λ_s value for FET in the normal region is smaller than that of BET in the inverted region, using eq 1 we derived the solvent reorganization energies of 1.53 and 2.16 eV for the forward and back ET, respectively, with the tunneling parameter (β) of 0.8 Å^{-1}, A = 0.35 in eq 1, for the stacked form and of 2.15 and 2.47 eV with the tunneling parameter of 1.0 Å^{-1} (A = 1.74) for the C-clamp form. The deduced coupling constants using eq 2 are ∼153 cm^{-1} for the stacked form and 32 cm^{-1} for the C-clamp form. The derived tunneling parameters (β) of 0.8 and 1.0 Å^{-1} for the stacked and C-clamp forms, respectively, are significant, clearly showing that the tunneling is not directly through water (β ∼1.6 Å^{-1} or A = 2.78). For the C-clamp form, the electron tunneling is also not directly through the covalent linker that consists of 3 C−N bonds and 4 C−C bonds with A = 2.28. For both cases of directly tunneling through water or the covalent linker, there are no meaningful solutions for the reorganization energies to meet both forward and back ET rates. Thus, the derived small tunneling parameters strongly suggest that both the forward and back ET dynamics are mediated by unique solvent molecules intervening between the donor and acceptor. For the stacked form (0.8 Å^{-1}), the ET is close to tunneling through a 4.0 Å covalent bond (0.71 Å^{-1}), and for the C-clamp form (1.0 Å^{-1}), the ET is like tunneling through a 7.0 Å β-sheet (1.0 Å^{-1}) in proteins.[57] Thus, some water molecules must be flanked by the donor and acceptor and are confined in the cleft of the partially folded C-clamp conformation. The MD simulations indicated some water molecules bridging the donor and acceptor in both the stacked and C-clamp configurations, as shown in Figure 9 for two snapshots corresponding to the two configurations with solvent mediation from our MD simulations.

In ACN solvent, the redox potentials of the donor and acceptor are slightly different from those in water and the free energies of ΔG_{FET} and ΔG_{BET} for the redox cycle are −0.93 and −3.2 eV, respectively.[64] The MD simulations also showed a possible folded C-clamp conformation with r_{DA} = 7.5 Å, slightly

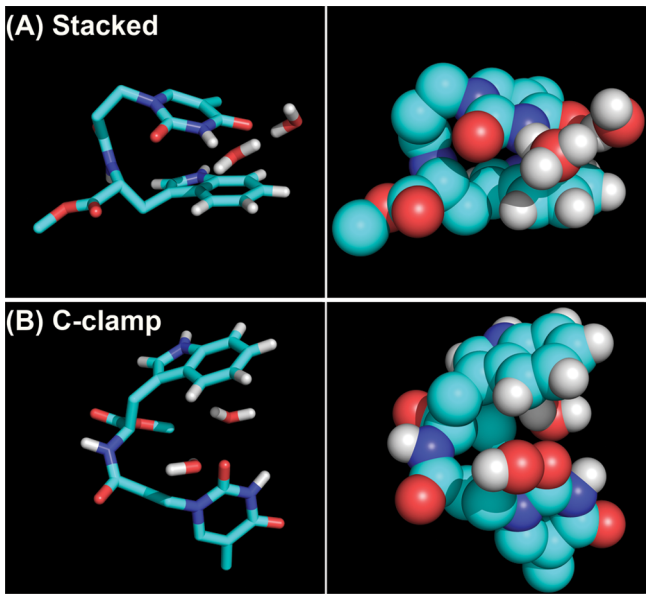

Figure 9. Two snapshots from our 25 ns MD simulations for the stacked (A) and C-clamp (B) conformations with possible mediated water molecules. In part A, two water molecules are bridged along two ring edges to enable all contacts at van der Waals distances. In part B, two water molecules intercalated in the cleft of the C-clamp configuration are linked with two rings to directly mediate electron tunneling.

dx.doi.org/10.1021/jp304518f | J. Phys. Chem. B 2012, 116, 9130−9140

more unfolded than the conformation in water. The solvent-assisted structure folding by ACN was also observed in an indo-linker-crown ether supramolecule.[65] With the measured forward and back ET rates, using eq 1, we derived the solvent reorganization energies of 1.97 and 2.3 eV with a tunneling parameter (β) of ~1.0 Å^{-1} (A = 1.95). The deduced coupling constant using eq 2 is ~25 cm^{-1}. The observed smaller λ_s values in ACN than in water follow the general trend with a decrease in solvent polarity. Similarly, the ACN molecules intercalated in the cleft must mediate the ET tunneling for both the forward and back ET processes, resulting in fast tunneling like through a 7.5 Å β-sheet in proteins with a tunneling parameter of 1.0 Å^{-1}.[57]

In nonpolar DIO solvent, the ET processes in the redox cycle become complicated. Also, the redox potentials of the donor and acceptor are unknown. Given the measured slow forward and fast back ET rates, there are no meaningful solutions in eq 1 at all for the solvent reorganization energies and driving forces for the forward and back ET processes considered together. One clear possibility is that, after the forward ET, the donor cation and acceptor anion attract each other and both ions can move together with a closer distance than the initial separation.[66] Assuming that the initial separation distance is similar to that in ACN at 7.5 Å and after the forward ET the final separation through attraction reaches about 3−4 Å, the contributions of the Coulombic interaction energies in eqs 3 and 4 are −0.87 eV for the forward ET and +(2.17−1.63) eV for the back ET. Under the conditions of knowing the forward and back ET rates and smaller λ_s values in nonpolar solvent and assumptions of the donor cation and acceptor anion attraction, we derived a set of the most meaningful solutions of the solvent reorganization energies, the difference of redox energies ($E_{ox} - E_{red}$) in nonpolar solvent DIO, and the tunneling scheme from eq 1 for the forward and back ET dynamics. For the slow forward ET of ~1 ns, the forward ET could tunnel through a similar C-clamp configuration as in ACN (r_{DA} = 7.5 Å) but with a larger tunneling parameter of 1.4 Å^{-1} (an α-helical type of tunneling scheme).[57] The forward reorganization energy is about ~0.6 eV and the final free energy is −0.1 eV, leading to the redox difference ($E_{ox} - E_{red}$) of ~4.9 eV, consistent with the trend that it should be larger in nonpolar solvent than that in polar solvent (3.1 eV in water). The observed smaller reorganization energy than that in polar solvent also follows the trend with a decrease in solvent polarity. However, it is larger than the estimated value (0.24 eV) from eq 5. The relatively larger value obtained in nonpolar DIO is consistent with a series of recent theoretical studies of ET in nonpolar solvents,[67−69] due to the polarized solvent molecules mainly in the first solvent shell induced by the large charge-separated donor−acceptor dipole. Significantly, due to the fast back ET (~100 ps), the derived *minimum* reorganization energy of the back ET after the cation−anion attraction with a separation of 3−4 Å for tunneling through mediation (1.4 Å^{-1}) is 1.45−1.79 eV. Clearly, the λ_s value of the back ET is significantly larger than the forward ET one, even with the final shorter distance through attraction. Thus, we believe that the high-frequency vibration effect is involved in the back ET, leading to an apparent larger λ_s value, as are schematically shown in Figure 10. Such vibrationally enhanced charge recombination has been observed in other chemical systems[24,70] and treated by the extended Sumi−Marcus ET model.[21−23] Also, the observed larger λ_s values of back ET in water and ACN could imply that the vibration excitation is involved in the back ET processes to

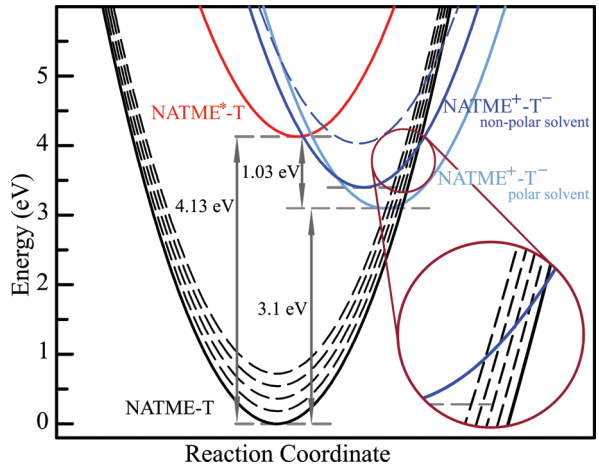

Figure 10. Schematic free energy profiles of the photoinduced redox cycle of NATME-T. The free energies of the forward and back ET are −1.03 and −3.10 eV, respectively. The dashed and solid dark blue curves represent the NATME$^+$-T$^-$ in nonpolar solvent immediately after the forward ET and subsequent attraction before the back ET, and for both curves, ΔG_{FET} and λ_S are smaller than those in polar solvent (see text). The inserted circle shows that the ground-state vibrational states are involved in the back ET reaction, effectively reducing the reaction barrier and enhancing the ET rates.

enhance the back ET rates. Thus, in nonpolar DIO solvent, the ET still tunnels through solvent mediation in the C-clamp configuration with a slow forward ET process. After charge separation, the two donor−acceptor ions attract together to a shorter distance. The subsequent charge recombination is then facilitated by the high-frequency donor/acceptor vibration coupling, resulting in the fast back ET.

Nonequilibrium Dynamics, Heterogeneous Configurations, and Conformation Fluctuations. We here focus on the forward ET dynamics on the partially folded C-clamp configuration in three solvents. Given that the solvation relaxations of three solvents are much faster than the ET processes, the observed stretched behaviors of the ET dynamics must result from the fluctuating distances between the donor and acceptor. Thus, the ET rate varies with the donor−acceptor distance and is time-dependent, i.e., $k_{ET} = k_{ET}(r,t)$. We can write such heterogeneous ET dynamics signal, $I_{ET}(t)$, by the following equation.

$$I_{ET}(t) = I_0 e^{-\int_0^t k(t')\,dt'} \tag{6}$$

Assuming that the conformations fluctuate in a harmonic potential, the distance between the donor and acceptor thus varies following $r_{DA} = r_e - r_a \cos(\omega t)$, where r_e and r_a are the donor−acceptor equilibrium distance and related fluctuating amplitude, respectively, in Å, and ω is the angular speed defined by $2\pi/\tau$ with a fluctuating oscillation period of τ in ps. Therefore, we can simplify the ET rate in eq 6 as follows.

$$k(t) = k_e e^{\beta r_a \cos(\omega t)},$$

$$\log k_e = 13 - 0.434\beta(r_e - r_0) - 3.1\frac{(\Delta G + \lambda)^2}{\lambda} \tag{7}$$

where k_e is the ET rate at the equilibrium distance (r_e). Substituting eq 7 into eq 6, we can obtain the $I_{ET}(t)$ expression as follows.

$$I_{ET}(t) = I_0 e^{-\int_0^t k_e e^{\beta r_a \cos(\omega t')}\,dt'} \tag{8}$$

dx.doi.org/10.1021/jp304518f | J. Phys. Chem. B 2012, 116, 9130−9140

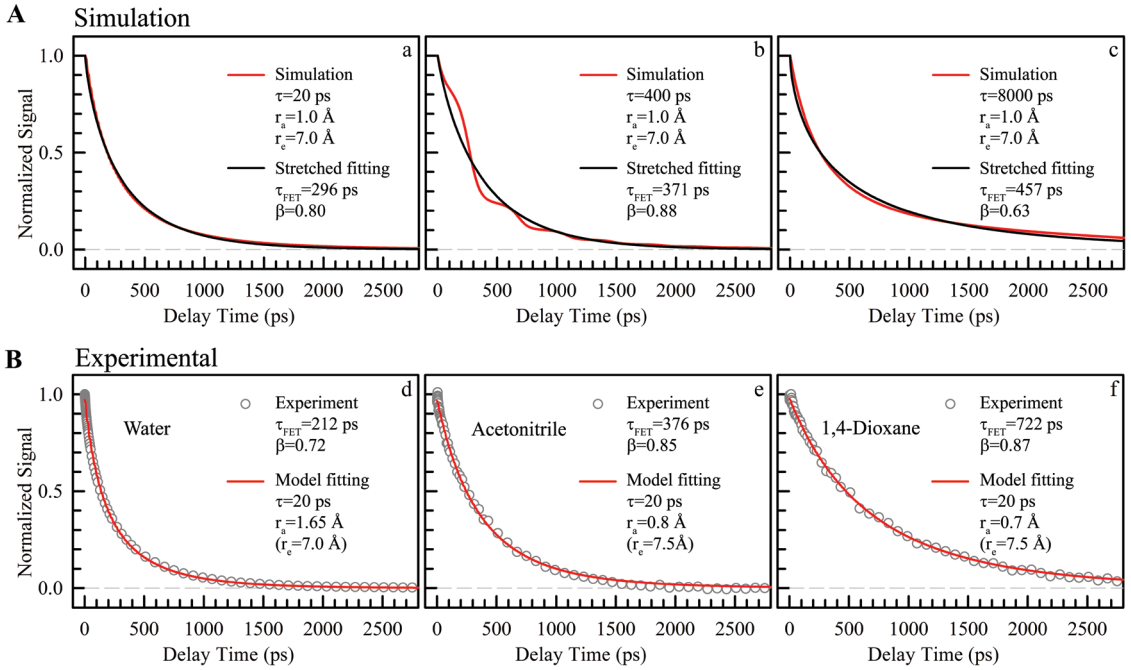

Figure 11. The nonequilibrium heterogeneous ET dynamics with the fluctuating C-clamp configuration. (A) A series of simulations (red curves) using eq 8 with a fluctuating period of τ = (a) 20 ps, (b) 400 ps, and (c) 8 ns at r_e = 7.0 Å and r_a = 1 Å with the stretched-exponential decay fitting (black curves); see text. (B) Three model fitting results (red curves) of the measured ET dynamics (gray circles) using eq 8 with the C-clamp conformations in three solvents to derive the actual fluctuating period (τ) and amplitude (r_a). r_e = 7.0 Å in water and r_e = 7.5 Å in acetonitrile and dioxane from our MD simulations. All k_e values in eq 8 are taken for our measurements in text.

We can perform numerical calculations on eq 8 to derive the ET dynamic behavior, or we can also use the Taylor expansion of the exponential term and rewrite eq 8 into the following expression.

$$I_{ET}(t) = (I_0 e^{-k_e t}) e^{-k_e[\beta r_a \sin(\omega t) + \beta^2 r_a^2[(2\omega t + \sin 2\omega t)/8\omega] + ...]} \quad (9)$$

The first term is a single-exponential decay with the rate at the equilibrium distance, and the second term is the correction term due to the conformation fluctuation around the equilibrium position. If the molecular structure is flexible as for NATME-T here, a distribution of molecular configurations is excited and such heterogeneous configurations would cause an overall stretched behavior. Figure 11A shows a series of simulation results calculated from eq 8 by an average of the ET dynamics assuming an initial distribution with a fluctuation potential energy of k_BT at r_a = 1.0 Å (r_e from the MD simulations). We took nine configurations with an interval of 0.4 Å at conformation fluctuation periods of τ = 20 ps, 400 ps, and 8 ns using the k_e value obtained in water. At each configuration, the population is weighted by the Boltzmann distribution and the initial rate is also considered by the initial distance (r). Clearly, all curves more or less follow a stretched behavior due to the initial heterogeneous configurations, and especially when the conformation fluctuates on the ultrafast (20 ps) or ultraslow (8 ns) time scale, relative to the ET dynamics, the ET dynamics nearly follows a stretched exponential decay (Figure 11A, a and c). Interestingly, when the fluctuation period of τ (400 ps) is on the similar time scale of the ET dynamics, an oscillatory stretched behavior would be observed (Figure 11A, b). Given the flexible NATME-T structure, the NATME-T could fluctuate on tens of picoseconds, faster than the ET dynamics, and Figure 11B shows the final fitting results for the three experimental forward ET dynamics in the three solvents using eq 8 with the derived k_e values and MD r_e distances in the previous section, convoluted with the lifetime contribution.

The fluctuation oscillation period of 20 ps is an approximation value, and the time period of less than 50 ps would give the similar results. Thus, the fluctuation period is in a few tens of picoseconds. Significantly, the fluctuation amplitudes (r_a) are 1.65 Å in water (Figure 11B, d), 0.8 Å in ACN (Figure 11B, e), and 0.7 Å in DIO (Figure 11B, f), directly following the trend of the fitted stretched parameter (β) values for the dynamics in three solvents. The more fluctuation, the more stretched behavior. The fluctuation harmonic potential is thus obtained, $V = k_BT((r - r_e)/r_a)^2$, with r_e and r_a corresponding to the derived values in three solvents. Clearly, in water, the fluctuation potential is flatter (r_a is much larger). Thus, for a flexible molecule, we can easily observe a stretched behavior of the nonequilibrium ET dynamics due to the flexible donor–linker–acceptor structure with initial heterogeneous configurations for photoinduced ET processes.

CONCLUSION

We reported here our systematic characterization of the forward ET (charge separation) and subsequent back ET (charge recombination) dynamics in a photoinduced redox cycle with a covalently single-bond-linked *N*-acetyl-tryptophan methyl ester (NATME) and thymine (T) flexible system. With femtosecond resolution, we precisely determined all the ET rates, forward and back, in three typical solvents with distinct polarities to examine how the structural flexibility and solvent polarity and configuration modulate the ET rates. Specifically, in water, we observed two distinct ET dynamics, one in hundreds of femtoseconds and the other in hundreds of picoseconds, corresponding to two different conformations.

dx.doi.org/10.1021/jp304518f | J. Phys. Chem. B 2012, 116, 9130–9140

One is a stacked configuration, and the other is a partially folded C-clamp structure (Figure 9). In polar acetonitrile and nonpolar dioxane, we only observed the ET dynamics in hundreds of picoseconds with a similar C-clamp configuration. The MD simulations showed these two possible configurations with large fluctuations. Significantly, with the C-clamp configuration, the observed forward ET dynamics in all three solvents follow a stretched-exponential behavior, directly reflecting heterogeneous conformations and the fluctuating nature of the flexible donor–linker–acceptor system. We simulated such fluctuating processes using a simple harmonic potential model and observed a fluctuating amplitude of 1.65 Å in water, 0.8 Å in acetonitrile, and 0.7 Å in dioxane with the fluctuating period in a few tens of picoseconds.

The back ET dynamics were observed in tens of picoseconds, much faster than the forward ET processes. With both the measured forward and back ET rates, we used the Marcus ET theory (semiempirical and semiclassical) and derived the solvent reorganization energies and coupling constants in three solvents. Significantly, we observed that, in the C-clamp configuration, the intervening solvent molecules in the C-clamp cleft strongly mediate electron tunneling with a tunneling parameter (β) of 1.0 $Å^{-1}$ in water and acetonitrile and 1.4 $Å^{-1}$ in dioxane. In nonpolar dioxane, after the forward ET, we observed that the cation donor and anion acceptor attract each other to a closer distance near van der Waals contact. For all ultrafast back ET, the results strongly suggest that the ground-state vibration coupling is involved in back ET, reduces the ET barriers, and enhances the back ET rates. The complete characterization of the forward and back ET dynamics together in the photoinduced redox cycle with a flexible donor–linker–acceptor system in three distinct solvent polarities provides an opportunity to study nonequilibrium ET processes with unique structural flexibility (C-clamp structural fluctuation) and intercalated solvent configuration to mediate electron tunneling.

AUTHOR INFORMATION

Corresponding Author

*E-mail: zhong.28@asc.ohio-state.edu.

Present Address

[†]Department of Chemistry, University of Science and Technology of China, Hefei 230026, PR China.

Notes

The authors declare no competing financial interest.

ACKNOWLEDGMENTS

This work was supported in part by the National Institute of Health (Grant GM074813), the National Science Foundation (Grant CHE0748358), the Camille Dreyfus Teacher-Scholar (to D.Z.). and the American Heart Association predoctoral fellowship (to Z.L.). We thank Prof. Sherwin Singer for helpful discussions and Drs. Chaitanya Saxena and Chen Zang for help with the initial experiment.

REFERENCES

(1) Barbara, P. F.; Meyer, T. J.; Ratner, M. A. *J. Phys. Chem.* **1996**, *100*, 13148–13168.

(2) Zimmt, M. B.; Waldeck, D. H. *J. Phys. Chem. A* **2003**, *107*, 3580–3597.

(3) Closs, G. L.; Miller, J. R. *Science* **1988**, *240*, 440–447.

(4) Wasielewski, M. R.; Niemczyk, M. P.; Johnson, D. G.; Svec, W. A.; Minsek, D. W. *Tetrahedron* **1989**, *45*, 4785–4806.

(5) Wasielewski, M. R. *Chem. Rev.* **1992**, *92*, 435–461.

(6) Warman, J. M.; Smit, K. J.; Jonker, S. A.; Verhoeven, J. W.; Oevering, H.; Kroon, J.; Paddonrow, M. N.; Oliver, A. M. *Chem. Phys.* **1993**, *170*, 359–380.

(7) Redmore, N. P.; Rubtsov, I. V.; Therien, M. J. *J. Am. Chem. Soc.* **2003**, *125*, 8769–8778.

(8) Saleh, N.; Kauffman, J. F. *J. Phys. Chem. A* **2004**, *108*, 7139–7146.

(9) Beratan, D. N.; Skourtis, S. S.; Balabin, I. A.; Balaeff, A.; Keinan, S.; Venkatramani, R.; Xiao, D. Q. *Acc. Chem. Res.* **2009**, *42*, 1669–1678.

(10) Skourtis, S. S.; Waldeck, D. H.; Beratan, D. N. *Annu. Rev. Phys. Chem.* **2010**, *61*, 461–485.

(11) Marcus, R. A.; Sutin, N. *Biochim. Biophys. Acta* **1985**, *811*, 265–322.

(12) Berlin, Y. A.; Grozema, F. C.; Siebbeles, L. D. A.; Ratner, M. A. *J. Phys. Chem. C* **2008**, *112*, 10988–11000.

(13) Closs, G. L.; Calcaterra, L. T.; Green, N. J.; Penfield, K. W.; Miller, J. R. *J. Phys. Chem.* **1986**, *90*, 3673–3683.

(14) Finckh, P.; Heitele, H.; Volk, M.; Michelbeyerle, M. E. *J. Phys. Chem.* **1988**, *92*, 6584–6590.

(15) Lewis, F. D.; Wagner-Brennan, J. M.; Denari, J. M. *J. Phys. Chem. A* **1998**, *102*, 519–525.

(16) Mataga, N.; Chosrowjan, H.; Taniguchi, S. *J. Photochem. Photobiol., C* **2005**, *6*, 37–79.

(17) Kumar, K.; Lin, Z.; Waldeck, D. H.; Zimmt, M. B. *J. Am. Chem. Soc.* **1996**, *118*, 243–244.

(18) Napper, A. M.; Read, I.; Waldeck, D. H.; Kaplan, R. W.; Zimmt, M. B. *J. Phys. Chem. A* **2002**, *106*, 4784–4793.

(19) Kauffman, J. F.; Khajehpour, M.; Saleh, N. *J. Phys. Chem. A* **2004**, *108*, 3675–3687.

(20) Chakrabarti, S.; Liu, M.; Waldeck, D. H.; Oliver, A. M.; Paddon-Row, M. N. *J. Phys. Chem. A* **2009**, *113*, 1040–1048.

(21) Sumi, H.; Marcus, R. A. *J. Chem. Phys.* **1986**, *84*, 4894–4914.

(22) Jortner, J.; Bixon, M. *J. Chem. Phys.* **1988**, *88*, 167–170.

(23) Barbara, P. F.; Walker, G. C.; Smith, T. P. *Science* **1992**, *256*, 975–981.

(24) Nagasawa, Y.; Yartsev, A. P.; Tominaga, K.; Bisht, P. B.; Johnson, A. E.; Yoshihara, K. *J. Phys. Chem.* **1995**, *99*, 653–662.

(25) Vauthey, E. *J. Phys. Chem. A* **2001**, *105*, 340–348.

(26) Lewis, F. D.; Kalgutkar, R. S.; Wu, Y. S.; Liu, X. Y.; Liu, J. Q.; Hayes, R. T.; Miller, S. E.; Wasielewski, M. R. *J. Am. Chem. Soc.* **2000**, *122*, 12346–12351.

(27) Mataga, N.; Kanda, Y.; Asahi, T.; Miyasaka, H.; Okada, T.; Kakitani, T. *Chem. Phys.* **1988**, *127*, 239–248.

(28) Kao, Y.-T.; Saxena, C.; Wang, L.; Sancar, A.; Zhong, D. *Proc. Natl. Acad. Sci. U.S.A.* **2005**, *102*, 16128–16132.

(29) Wang, H.; Lin, S.; Allen, J. P.; Williams, J. C.; Blankert, S.; Laser, C.; Woodbury, N. W. *Science* **2007**, *316*, 747–750.

(30) Li, J.; Liu, Z.; Tan, C.; Guo, X.; Wang, L.; Sancar, A.; Zhong, D. *Nature* **2010**, *466*, 887–890.

(31) Liu, Z.; Tan, C.; Guo, X.; Kao, Y. T.; Li, J.; Wang, L.; Sancar, A.; Zhong, D. *Proc. Natl. Acad. Sci. U.S.A.* **2011**, *108*, 14831–14836.

(32) Chang, C.-W.; Guo, L.; Kao, Y.-T.; Li, J.; Tan, C.; Li, T.; Saxena, C.; Liu, Z.; Wang, L.; Sancar, A.; Zhong, D. *Proc. Natl. Acad. Sci. U.S.A.* **2010**, *107*, 2914–2919.

(33) Chang, C.-W.; He, T.-F.; Guo, L.; Stevens, J. A.; Li, T.; Wang, L.; Zhong, D. *J. Am. Chem. Soc.* **2010**, *132*, 12741–12747.

(34) Qiu, W.; Wang, L.; Lu, W.; Boechler, A.; Sanders, D. A. R.; Zhong, D. *Proc. Natl. Acad. Sci. U.S.A.* **2007**, *104*, 5366–5371.

(35) Qiu, W.; Li, T.; Zhang, L.; Yang, Y.; Kao, Y.-T.; Wang, L.; Zhong, D. *Chem. Phys.* **2008**, *350*, 154–164.

(36) Wu, D.; Hu, Q.; Yan, Z.; Chen, W.; Yan, C.; Huang, X.; Zhang, J.; Yang, P.; Deng, H.; Wang, J.; Deng, X.; Shi, Y. *Nature* **2012**, *484*, 214–219.

(37) Christie, J. M.; Arvai, A. S.; Baxter, K. J.; Heilmann, M.; Pratt, A. J.; O'Hara, A.; Kelly, S. M.; Hothorn, M.; Smith, B. O.; Hitomi, K.; Jenkins, G. I.; Getzoff, E. D. *Science* **2012**, *335*, 1492–1496.

(38) Kao, Y.-T.; Tan, C.; Song, S. H.; Ozturk, N.; Li, J.; Wang, L.; Sancar, A.; Zhong, D. *J. Am. Chem. Soc.* **2008**, *130*, 7695–7701.

(39) Kao, Y.-T.; Saxena, C.; He, T.-F.; Guo, L.; Wang, L.; Sancar, A.; Zhong, D. *J. Am. Chem. Soc.* **2008**, *130*, 13132−13139.
(40) Stubbe, J.; Nocera, D. G.; Yee, C. S.; Chang, M. C. Y. *Chem. Rev.* **2003**, *103*, 2167−2201.
(41) Kim, S. T.; Hartman, R. F.; Rose, S. D. *Photochem. Photobiol.* **1990**, *52*, 789−794.
(42) Song, Q.-H.; Tang, W.-M.; Hei, X.-M.; Wang, H.-B.; Guo, Q.-X.; Yu, S.-Q. *Eur. J. Org. Chem.* **2005**, 1097−1106.
(43) Kao, Y.-T.; Song, Q.-H.; Saxena, C.; Wang, L.; Zhong, D. *J. Am. Chem. Soc.* **2012**, *134*, 1501−1503.
(44) Zhang, L.; Kao, Y.-T.; Qiu, W.; Wang, L.; Zhong, D. *J. Phys. Chem. B* **2006**, *110*, 18097−18103.
(45) Reichardt, C. *Solvents and Solvent Effects in Organic Chemistry*, 3rd ed.; Wiley: Weinheim, Germany, 2003.
(46) Lide, D. R. *CRC Handbook of Chemistry and Physics*, 84th ed.; CRC Press: Boca Raton, FL, 2003.
(47) Petrich, J. W.; Chang, M. C.; Mcdonald, D. B.; Fleming, G. R. *J. Am. Chem. Soc.* **1983**, *105*, 3824−3832.
(48) Szabo, A. G.; Rayner, D. M. *J. Am. Chem. Soc.* **1980**, *102*, 554−563.
(49) Ricci, R. W.; Nesta, J. M. *J. Phys. Chem.* **1976**, *80*, 974−980.
(50) Peon, J.; Zewail, A. H. *Chem. Phys. Lett.* **2001**, *348*, 255−262.
(51) Middleton, C. T.; de La Harpe, K.; Su, C.; Law, Y. K.; Crespo-Hernandez, C. E.; Kohler, B. *Annu. Rev. Phys. Chem.* **2009**, *60*, 217−239.
(52) Defelippis, M. R.; Murthy, C. P.; Broitman, F.; Weinraub, D.; Faraggi, M.; Klapper, M. H. *J. Phys. Chem.* **1991**, *95*, 3416−3419.
(53) Scannell, M. P.; Fenick, D. J.; Yeh, S. R.; Falvey, D. E. *J. Am. Chem. Soc.* **1997**, *119*, 1971−1977.
(54) Ragone, R.; Colonna, G.; Servillo, L.; Irace, G. *Photochem. Photobiol.* **1985**, *42*, 505−508.
(55) Jovanovic, S. V.; Steenken, S. *J. Phys. Chem.* **1992**, *96*, 6674−6679.
(56) Page, C. C.; Moser, C. C.; Chen, X. X.; Dutton, P. L. *Nature* **1999**, *402*, 47−52.
(57) Gray, H. B.; Winkler, J. R. *Proc. Natl. Acad. Sci. U.S.A.* **2005**, *102*, 3534−3539.
(58) Rehm, D.; Weller, A. *Isr. J. Chem.* **1970**, *8*, 259−271.
(59) Nunthaboot, N.; Tanaka, F.; Kokpol, S.; Chosrowjan, H.; Taniguchi, S.; Mataga, N. *J. Photochem. Photobiol., A* **2009**, *201*, 191−196.
(60) Tang, W.-J.; Guo, Q.-X.; Song, Q.-H. *J. Phys. Chem. B* **2009**, *113*, 7205−7210.
(61) Gould, I. R.; Farid, S. *Acc. Chem. Res.* **1996**, *29*, 522−528.
(62) Eberson, L. *Adv. Phys. Org. Chem.* **1982**, *18*, 79−185.
(63) Asahi, T.; Ohkohchi, M.; Matsusaka, R.; Mataga, N.; Zhang, R. P.; Osuka, A.; Maruyama, K. *J. Am. Chem. Soc.* **1993**, *115*, 5665−5674.
(64) Seidel, C. A. M.; Schulz, A.; Sauer, M. H. M. *J. Phys. Chem.* **1996**, *100*, 5541−5553.
(65) Lu, W.; Qiu, W.; Kim, J.; Okobiah, O.; Hu, J.; Gokel, G. W.; Zhong, D. *Chem. Phys. Lett.* **2004**, *394*, 415−422.
(66) Tachiya, M.; Seki, K. *J. Phys. Chem. A* **2007**, *111*, 9553−9559.
(67) Leontyev, I. V.; Tachiya, M. *J. Chem. Phys.* **2005**, 123.
(68) Gupta, S.; Matyushov, D. V. *J. Phys. Chem. A* **2004**, *108*, 2087−2096.
(69) Matyushov, D. V.; Schmid, R. *Mol. Phys.* **1995**, *84*, 533−552.
(70) Gladkikh, V.; Burshtein, A. I.; Feskov, S. V.; Ivanov, A. I.; Vauthey, E. *J. Chem. Phys.* **2005**, 123.